Journal of Ayurveda and Integrative Medicine 15 (2024) 100986

Contents lists available at ScienceDirect

Journal of Ayurveda and Integrative Medicine

journal homepage: elsevier.com/locate/jaim

In-silico evaluation of *Oroxylum indicum* vent compounds in the plausible treatment and prevention of nasopharyngeal cancer

Saketh Ram Thrigulla [a], Gagandeep Singh [b,*], Hemant Soni [b], Smriti Tandon [b], Shruti Koulgi [c], Mallikarjunachari V.N. Uppuladinne [c], Vinod Jani [c], Uddhavesh Sonavane [c], Rajendra Joshi [c], Yashika Gandhi [d], Vijay Kumar [d], Vaibhav Charde [e], Sujeet K. Mishra [d], Mukesh Chincholikar [f], Rakesh Narayan [f], Vinod Lavaniya [f], Ch Venkata Narasimhaji [d], Narayanam Srikanth [f], Rabinarayan Acharya [f]

[a] *Ayush Grid Cell, Ministry of Ayush, Government of India, India*
[b] *Section of Microbiology, Central Ayurveda Research Institute, Jhansi, CCRAS, Ministry of Ayush, India*
[c] *High Performance Computing - Medical and Bioinformatics Applications Group, Centre for Development of Advanced Computing (C-DAC), Panchawati, Pashan, Pune, 411008, India*
[d] *Section of Chemistry, Central Ayurveda Research Institute, Jhansi, CCRAS, Ministry of Ayush, India*
[e] *Section of Pharmacy, Central Ayurveda Research Institute, Jhansi, CCRAS, Ministry of Ayush, India*
[f] *Central Council for Research in Ayurvedic Sciences, Ministry of Ayush, India*

ARTICLE INFO

Keywords:
Oroxylum indicum vent
Epstein barr virus (EBV)
Nasopharyngeal carcinoma (NPC)
Baicalein
Molecular docking
MD simulation

ABSTRACT

Background: Shyonaka (*Oroxylum indicum* Vent) is widely used in Ayurveda and in ethnomedical practice for the treatment of inflammation, pain, diarrhea, non-healing ulcers, and cancer. Owing to the high prevalence of Epstein-Barr virus (EBV) infection in Nasopharyngeal carcinoma (NPC) patients, simultaneous targeting of proteins involved in both EBV replication and NPC proliferation might help to manage the disease effectively.
Objectives: This study is designed to identify potential dual targeting inhibitors from *Oroxylum indicum* having the potential to inhibit both EBV and NPC. This study also attempted quantitative analysis of Shyonaka Bark Decoction (SBD) to confirm the presence of Baicalein and Chrysin which are predominant marker compounds of Shyonaka.
Methodology: The HPLC analysis of stem bark and root bark of *Oroxylum indicum* was done to estimate the presence of marker compounds Baicalein and Chrysalin. The in-silico analysis included ADMET analysis followed by molecular docking of known compounds from *Oroxylum indicum* (retrieved from IMPPAT database) onto the target proteins of EBV (BHRF1, NEC1, dUTPase, Uracil DNA glycosylase) and NPC (COX-2, EGFR, and MDM2) using DOCK6 tool. Further validations were done using the molecular dynamics simulations of top screened molecules onto the selected target proteins using AMBER20 package and their corresponding MMGBSA binding free-energy values were calculated.
Results: The molecular docking revealed that the key molecules from the plant, scutellarein 7-rutinoside (S7R), scutellarin (SCU) and 6-hydroxyluteolin, Baicalein and 5,7-Dihydroxy-2-phenyl-6-[3,4,5-trihydroxy-6-(hydroxymethyl)oxan-2-yl]oxychromen-4-one (57D) are effectively intervening with the target proteins of EBV, one of the key causative factors of NPC and the NPC specific targets which have the potential to reduce tumor size and other consequences of NPC. The molecular dynamics simulations of S7R, Baicalein and 57D, Baicalein with MDM-2 protein and dUTPase protein, respectively, showed stable interactions between them which were further assessed by the binding energy calculations.
Conclusion: Overall, the in-silico evaluation of these phytochemicals with target proteins indicates their potential to inhibit both EBV and NPC which needs further in-vitro and in-vivo validations.

Peer review under responsibility of Transdisciplinary University, Bangalore.
* Corresponding author. Assistant Research officer (Biotechnology) Central Ayurveda Research Institute, Jhansi, CCRAS, Ministry of Ayush, Govt. of India, India.
E-mail addresses: Gagandeep.ccras@nic.in, Gagan.sk.1994@gmail.com, gsk.ccras@gmail.com (G. Singh).

https://doi.org/10.1016/j.jaim.2024.100986
Received 12 September 2023; Received in revised form 4 May 2024; Accepted 17 May 2024

Table 1
Properties of Shyonaka (*Oroxylum indicum* Vent.) as described in Ayurvedic literature.

Rasa (taste)	Madhura (Sweet), Tikta (bitter), Kaṣhaya (astringent)
Guna (qualities)	Laghu (light),Ruksha (dry)
Virya (potency)	Shita (cold) [mentioned as Ushna (hot) in Dravyaguna Vijnana by Dr. Priyavrata Sharma]
Vipaka (post digestive state)	Katu (pungent)
Karma(activities)	Kaphavatashamaka (pacifies *Kapha,* and *Vata*), Dipana (digestion and metabolism enhancing), Grahi (absorptive)
Ganna (therapeutic group)	Group of ten unctuous enema assisting substance (anuvasanopaga-mahakashaya, SAT-F.213), group of ten intestinal astringent dravya (purishasamgrahaṇiya-mahakashaya, SAT-F.218), group of ten anti-phlogistic/anti-inflammatory substances (shvayathuhara-mahakashaya, SAT-F.225) and group of ten calafacient, a drug or other substance that gives a sensation of warmth (shitaprashamana-mahakashaya, SAT-F.229)
Therapeutic Uses	*Vatatisara* (a type of diarrhea), Kasa (cough), *Aruchi* (tastelessness), *Basti Roga* (diseases of urinary bladder), *Amavata* (a type of rheumatism), *Udara Roga* (ascites), *Urustambha* (stiff thigh), *Vatavyadhi* (disorders due to *Vata*), *Karna Roga* (diseases of ear), *Shotha* (oedema/inflammation), *Gulma* (lump), *Arsha* (haemorrhoids), *Krimi* (worm infestation), *Granthi* (cyst), *Nasaroga* (diseases of nose), *Vrana* (wound), *Sannipataja Jwara* (a type of fever)
References of Shyonaka in the context of *Granthi, Shotha, Uroroga, Nasaroga* etc.	1. Shyonaka has been mentioned as one of the ingredients of *Himsradi lepa* (indicated in *Vataja Granthi*) in the chapter of *Sushrutasamhita* titled *Granthyapachyarbudagalagandachikitsa*. 2. It is one of the ingredients of various groups of drugs such as *ShwayatuharaMahakashaya and Rodhradi gana, Viratarvadi gana.* 3. It is one among the ingredient of *Chyavanaprasha&Brahmarasayana* mainly used in *Kasa (cough)*, *Shvasa* (difficulty in breathing)& also in *Svarakshaya* (feeble voice), *Uroroga* (diseases of chest region) *4. Shyonaka* is an ingredientof *Shatahvadi dhoomavarti* which isuseful in *Vataja Pinasa* (a type of nose disease)
Important Formulations	*Dashamula Kvatha Churna*, *Amritarishta*, *Dantyadyarishta*, *Dashamularishta*, *Narayana taila*, *Dhanavantara Ghrita*, *Brahma Rasayana*, *Chyavanaprasha Awaleha*
Dose	5–10 g. in powder form 25–50 g. in decoction.
Rasa (taste)	Madhura (Sweet), Tikta (bitter), Kasshaya (astringent)
Guna (qualities)	*Laghu* (light), *Ruksha* (dry)
Virya (potency)	*Shita* (cold) [mentioned as Ushna (hot) in Dravyaguna Vijnana by Dr. Priyavrata Sharma]
Vipaka (Post digestive state)	Kattu (pungent)
Karma:(activities)	*Kaphavatashamaka* (pacifies *Kapha*, and *Vata*), *Dipana* (digestion and metabolism enhancing), *Grahi* (absorptive)
Ganna (ther apeutic group)	Group of ten unctuous enema assisting substance (*anuvasanopaga-mahakashaya*, SAT-F.213), group of ten intestinal astringent dravya (*purishasamgrahaṇiya-mahakashaya*, SAT-F.218), group of ten anti-phlogistic/anti-inflammatory substances (*shvayathuhara- mahakashaya*, SAT-F.225) and group of ten calafacient, a drug or other substance that gives a sensation of warmth (*shitaprashamana- mahakashaya*, SAT-F.229)
Therapeutic Uses:	*Vatatisara* (a type of diarrhea), *Kasa* (cough), *Aruchi* (tastelessness), *Basti Roga* (diseases of urinary bladder), *Amavata* (a type of rheumatism), *Udara Roga* (ascites), *Urustambha* (stiff thigh), *Vatavyadhi* (disorders due to Vata), *Karna Roga* (diseases of ear), *Shotha* (oedema/inflammation), *Gulma* (lump), *Arsha* (haemorrhoids), *Krimi* (worm infestation), *Granthi* (cyst), *Nasaroga* (diseases of nose), *Vrana* (wound), *Sannipataja Jwara* (a type of fever)
References of Shyonaka in the context of *Granthi, Shotha, Uroroga, Nasaroga* etc.	1. Shyonaka has been mentioned as one of the ingredients of Himsradi lepa (indicated in Vataja Granthi) in the chapter of Sushruta samhita titled Granthya pachyar budagalaganda chikitsa. 2. It is one of the ingredients of various groups of drugs such as Shwayatuhara Mahakashaya and Rodhradi gana, Viratarvadi gana. 3. It is one among the ingredient of *Chyavanaprasha* & *Brahmarasayana* mainly used in Kasa (cough), Shvasa (difficulty in breathing) & also in Svarakshaya (feeble voice), Uroroga (diseases of chest region) 4. Shyonaka is an ingredient of Shatahvadi dhoomavarti which is useful in Vataja Pinasa (a type of nose disease)
Important Formulations	Dashamula Kvatha Curna, Amritarishta, Dantyadyarishta, Dashamularishta, Narayana taila, Dhanavantara Ghrita, Brahma Rasayana, Chyavanaprasha Awaleha
Dose	5–10 g. in powder form 25–50 g. in decoction.

1. Introduction

Application of Shyonaka (*Oroxylum indicum* Vent.) is very common in Ayurvedic and ethnomedicinal practice for the treatment of inflammation, pain, wound healing, diarrhea and cancer [1,2]. The details of Ayurvedic usage of Shyonaka are mentioned in Table 1 [3–14].

1.1. Application of Shyonaka in the treatment of cancer: Leads from in-vitro to in-vivo experiments and a case study

Many groups have identified the effectiveness of *Oroxylum indicum* Vent extracts against multiple cancer types including Ehrlich's ascites carcinoma [15], breast cancer [16], epidermoid carcinoma of the larynx (Hep2 cell lines) [17], and Nasopharyngeal carcinoma [1,18]. In another reported case study (1999) [1], a patient from Senapati district of Manipur suffering from Nasopharyngeal carcinoma (NPC) underwent multiple chemotherapies but could not be cured. Later, on recommendation of a fellow Tangkhul Naga tribe person whose relative got cured of NPC by consuming the decoction of *Oroxylum indicum* Vent bark, the patient was also administered the same treatment. About 1.0 kg of fresh bark was boiled in 5 L of water for 30–40 min and the decoction was filtered in a bottle. A teacup (~100 ml) of this decoction alone or with honey was administered orally three times a day to the patient. The honey was added to the decoction to neutralize the bitter taste. After 2 weeks of the treatment the patient was found to be free from the pain with gradual reduction in swelling of the face and alleged to be cured from NPC.

1.2. Incidence of nasopharyngeal carcinoma (NPC)

Head and neck cancer is the major form of cancer prevalent in India. NPC is one type of cancer which shows marked geographic differences, with highest incidence rates in Southern China and in few north eastern states of India viz., Nagaland and Manipur. Further, it is pertinent to note that, the prevalence of NPC has decreased by roughly 30% in some endemic regions over the past 20 years. It might be because of environmental changes or lifestyle adaptation of the local population [19–21]. The GLOBOCON 2020 estimated 1,33,354 (0.7%) new cases for nasopharyngeal carcinoma. The incidence (cases, age-standardized rate, cumulative risk) and mortality data (deaths, age-standardized rate, cumulative risk) are mentioned in Tables 2 and 3 [22].

As evident from the previous literature, NPC exhibits a very substantial connection with Epstein-Barr virus (EBV) infection. In terms of the treatment regime, radiation therapy is typically effective in treating

Table 2
Global incidence of nasopharyngeal carcinoma (NPC)

Males			Females		
Cases	Age- Standardized Rate (Global)	Cumulative Risk, Ages 0–74 Years, %	Cases	Age- Standardized Rate (Global)	Cumulative Risk, Ages 0–74 Years, %
96,371	2.2	0.24	36,983	0.8	0.09

Table 3
Global deaths due to nasopharyngeal carcinoma (NPC)

Males			Females		
Cases	Age- Standardized Rate (Global)	Cumulative Risk, Ages 0–74 Years, %	Cases	Age- Standardized Rate (Global)	Cumulative Risk, Ages 0–74 Years, %
58,094	1.3	0.16	21,914	0.5	0.05

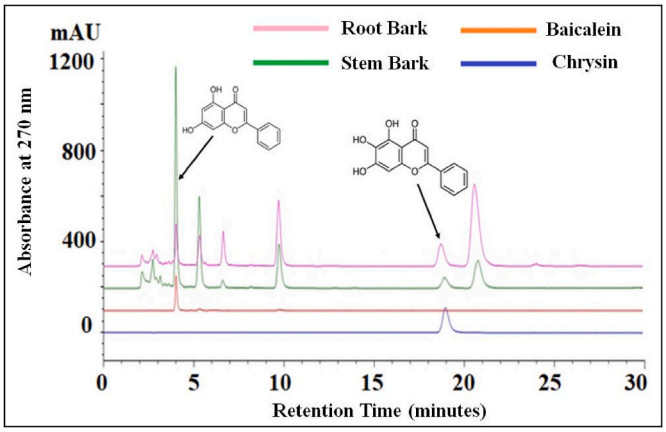

Fig. 1. HPLC analysis of root and stem bark extracts of *O. indicum* and standards (Baicalein and Chrysin) at 270 nm.

nasopharyngeal cancer. The clinical outcome has significantly improved over time as a result of more precise staging and better treatment procedures, however, NPC's distinctive and frequently misleading histological characteristics have led to debates about the tumor's nature and continue to be a challenge for surgical pathologists [23].

1.3. Chemical profile of Oroxylum indicum vent

So far, the following chemicals have been isolated from various parts of *O. indicum* Vent [2,24,25]. The list is as follows: 4-Hydroxycinnamic acid (bark), 5,7-Dihydroxy-2-phenyl-6-[3,4,5-trihydroxy-6-(hydroxymethyl)oxan-2-yl]oxychromen-4-one (seed), 6-Hydroxyluteolin (bark), Aloe emodin (leaf), Anthraquinone (leaf), Apigenin 7,4′-dimethyl ether (bark), Baicalein (root, bark, leaf, stem, seed), Baicalein 6-glucoside (seed), Baicalein (leaf, seed), beta-Sitosterol (bark, root, seed, wood), biochanin A (root), Chrysin (bark, leaf, root, stem), Dihydrobaicalein (bark), Dimethyl terephthalate (root), Ellagic acid (root), Flavanone, 5, 7-dihydroxy-6-methoxy-gamma-Tocopherol (bark, seed), Hispidulin (root), Lauric acid (seed), Linoleic acid (seed), Myristic acid (seed), Nepetin (bark), Octanoic acid (seed), Oleic acid (seed), Oroxindin (root, seed), Oroxylin A (bark), Palmitic acid (seed), Palmitoleic acid (seed), Prunetin (wood), Scutellarein (bark, leaf), Scutellarein 7-rutinoside (bark), Scutellarin (bark, leaf) and, Stearic acid (seed).

2. Material and methods

2.1. Sample preparation and HPLC analysis

The root and stem barks of *Oroxylum indicum* Vent were collected from the garden of CARI Jhansi and authenticated by the botany section (CARI Jhansi) with accession number Mus/O8/Wp. The plant name was cross-checked with Global Biodiversity Information Facility (https://www.gbif.org/species/4090936).

The HPLC analysis of stem bark and root bark of *O. indicum* was performed by using the method reported [26] with minor modifications, where marker compounds Baicalein and Chrysin were quantitatively identified. In brief, 5 g of the powdered sample (stem bark or root bark) and 50 mL of methanol was taken in 250 mL beaker, sonicated for 15 min and was then centrifuged at 5000 rpm for 5 min. The resultant supernatant upon filtration by 0.22-μm syringe filter was used as the sample solution for HPLC analysis. HPLC analysis was carried out using an Agilent 1260 Infinity II LC system (Agilent Technologies), equipped with a Multicolumn thermostat (MCT), autosampler, flexible pump, 100 μL syringe, and Diode Array Detector (DAD) with wavelength range 200–800 nm and the data was analyzed on OpenLab CDS ChemStation Edition software. The chromatographic conditions include C18 (4.6 × 250 mm, 5μ particle size) column as stationary phase, Water (0.1 % Formic acid): Methanol: Acetonitrile (47: 28: 25 v/v/v) as mobile phase with 1.0 mL/min flow rate, injection volume of 5 μL, and 30 °C MCT temperature. The targeted phytochemicals (baicalein and chrysin) in, stem bark or root bark were analyzed at 270 nm.

Table 4
The list of important target proteins from *Homo sapiens* and Epstein Barr Virus (EBV) used in this study.

	EBV Target Proteins			Cancer Target Proteins		
S. No.	Target Name	RCSB PDBID	Role of Target Protein	Target Name	RCSB PDBID	Role of Target Protein
1.	BHRF1	*7P33*	Inhibits pro-apoptotic proteins and responsible for chemo-resistance and lymphomagenesis.	COX-2	5KIR	Involved in inflammatory and neoplasmic activities (NPC migration and invasiveness).
2.	NEC1	7T7I	Responsible for virion nuclear egress in association with NEC2.	EGFR	1M17	Enhances EBV infection and promotes EBV metastasis.
3.	dUTPase	2BT1	Involved in lytic cycle and reactivation of EBV in infected cell and modulate the immune response.	MDM2	4IPF	Negatively regulates p53 and a potential target involved in NPC.
4.	Uracil DNA Glycosylase	2J8X	Crucial for viral replication.	–	–	–

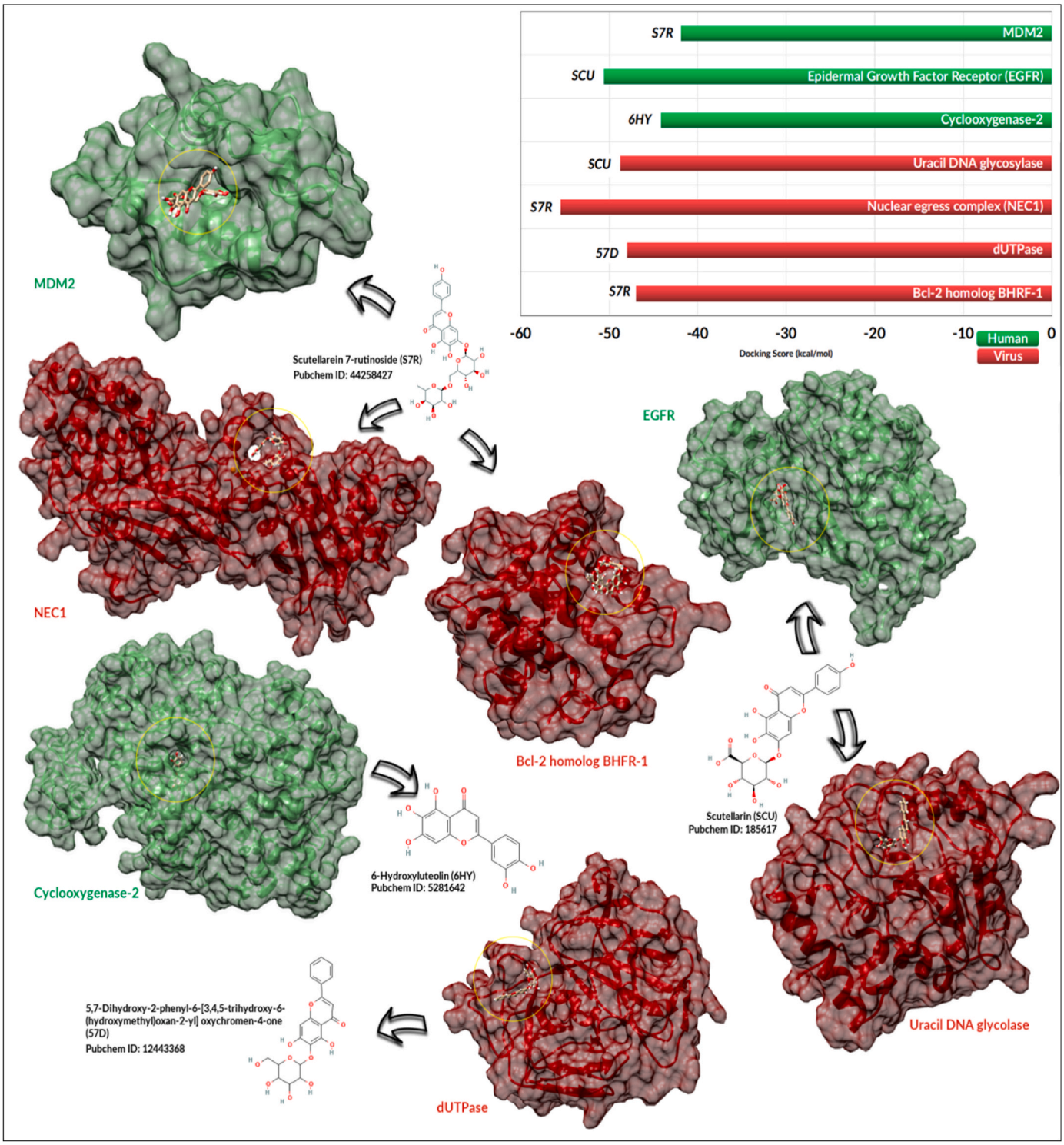

Fig. 2. Bar plot shows the docking scores for the best docked phytochemical for the three human (MDM2, EGFR, cyclooxygenase-2) (shown in green) and four viral (Uracil DNA glycosylase, NEC1, dUTPase, Bcl-2 homolog BHRF1) (shown in red) proteins. Chemical structures of phytochemicals pointing towards the protein they were found to be best bound.

2.2. Molecular docking

The docking of the phytochemicals against three human proteins (MDM2, EGFR, and cyclooxygenase-2) and four viral proteins (Uracil DNA glycosylase, NEC1, dUTPase, and Bcl-2 homolog BHRF1) was performed using the DOCK6 tool [27]. The receptor parameters for all proteins were generated using UCSF Chimera [28]. The AMBER14SB force field was used for parameterization [29]. This was followed by identification of the active site using the sphgen module of DOCK6. Spheres were generated on the surface of the receptor molecule and the cluster of the spheres around the coordinates of the pre-bound ligand was considered as the active site. This was followed by generation of grid over the active site, in order to effectively accommodate the ligand molecule. This was performed by the grid module of DOCK 6. The last step was docking of the phytochemicals to the prepared receptors; it was performed by dock6 module of DOCK 6. Apart from the phytochemical

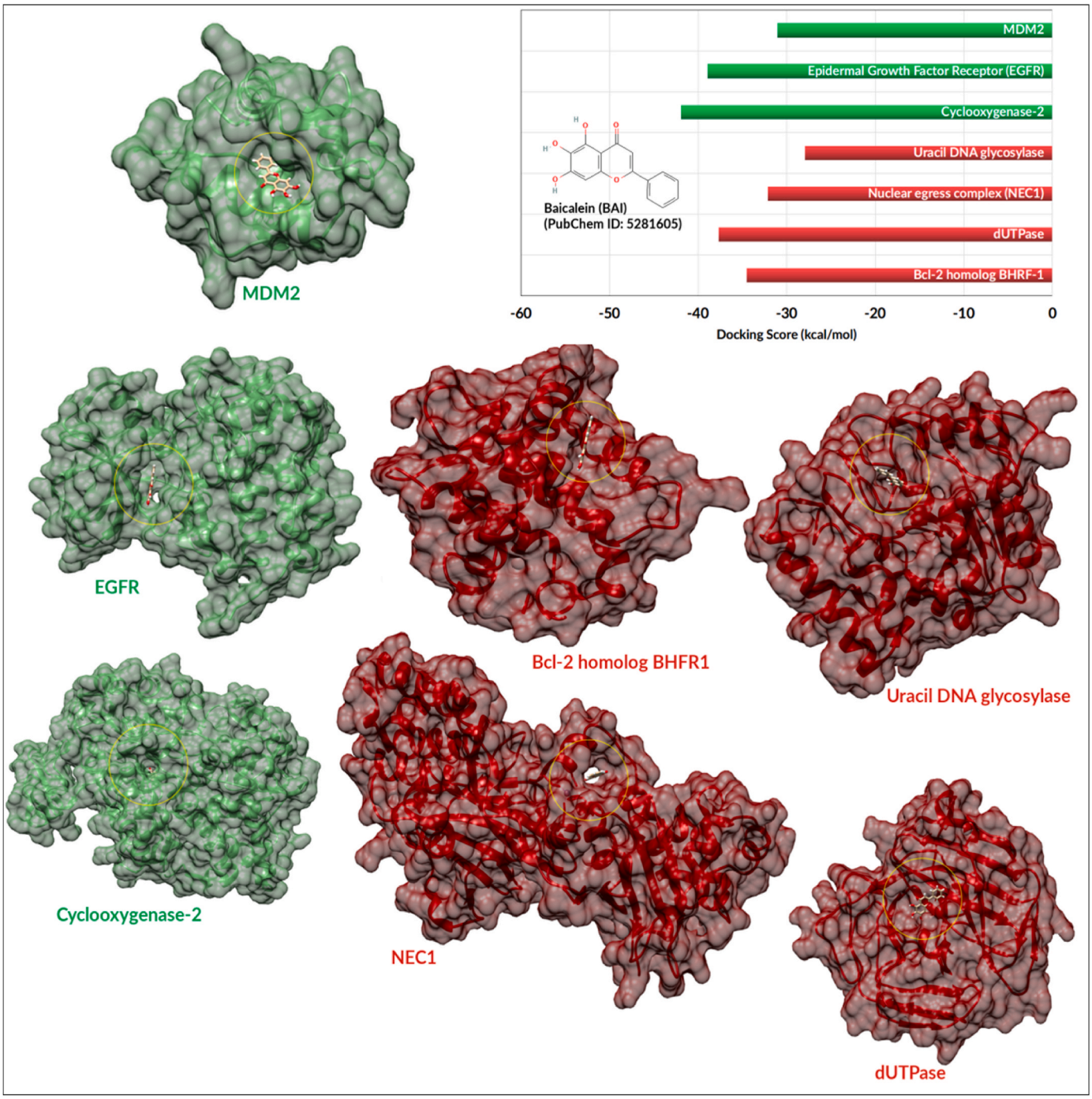

Fig. 3. Bar plot shows the docking scores for baicalein against the three human (MDM2, EGFR, cyclooxygenase-2) (shown in green) and four viral (Uracil DNA glycosylase, NEC1, dUTPase, Bcl-2 homolog BHRF1) (shown in red) proteins. (Inset) 2D representation of Baicalein molecule beside the bar plot.

docking on to the selected receptors, co-crystal docking was also carried out to check the accuracy of the docking process. The pre-bound ligand of the crystal structure was removed and then the ligand was docked onto the same receptor with above mentioned protocol of docking. The structures of best scored protein-ligand complexes and the docking scores are reported. Two protein-ligand complexes namely, MDM2-S7R and dUTPase-57D are subjected for molecular dynamics simulations. One of the important phytochemical baicalein was also docked against all the seven protein targets. Baicalein-bound complexes MDM2-BAI and dUTPase-BAI were also subjected for MD simulations.

2.3. Molecular dynamics simulations

Best scoring phytochemicals were selected for the molecular dynamics simulations with proteins (MDM2-S7R, dUTPase-57D). Also, simulations using two baicalein bound protein complexes namely, MDM2-BAI, dUTPase-BAI was carried out. The simulations were performed using the AMBER 20 simulation package [30]. The AMBER FF14SB force field was used for generation of the parameters for proteins [29]. The antechamber module of AMBERTOOLS along with the GAFF force field was used to generate the parameters for phytochemicals [31, 32]. The systems were neutralized by Na+/Cl-ions and solvated using the TIP3P water model. The minimization was performed for 20,000

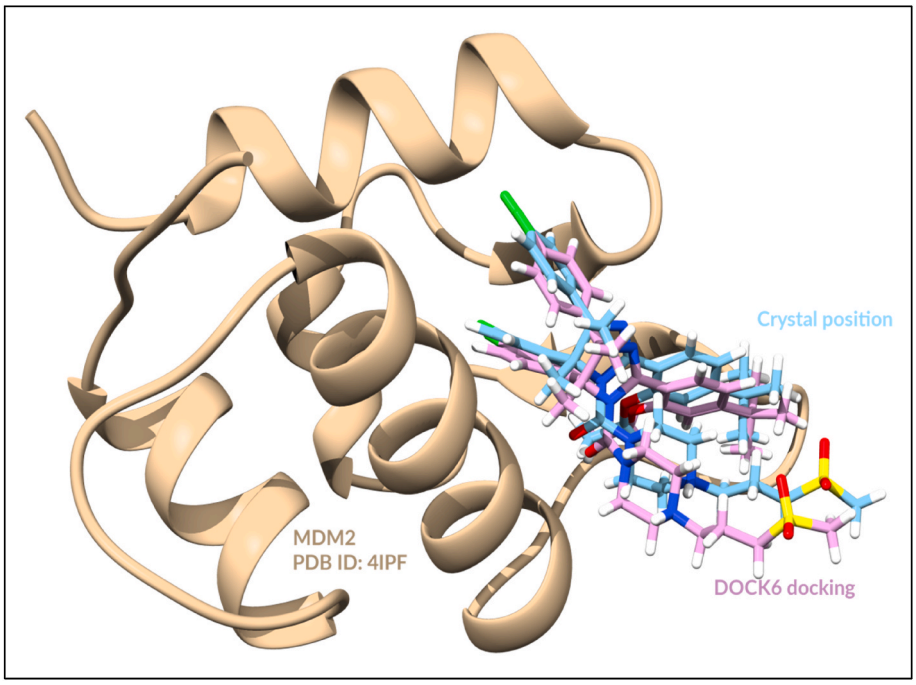

Fig. 4. Superimposition of MDM2 (PDB ID: 4IPF) and docked MDM2 with the crystal ligand.

Table 5
Drug likeliness properties calculated for S7R(a), 6HY(b), 57D(c), SCU(d) and BAI(e).

PubChem ID	Mol. wt. (g/mol)	No. of H-bond acceptors	No. of H-bond donors	Total Surface Area (Å^2)	Lipophilicity (WLOGP)	Solubility	GI absorption	BBB permeability	Pgp substrate	CYP3A4 Inhibitor	log Kp (cm/s)	Lipinski violations
[a]44258427	594.52	15	9	249.20	−1.39	Soluble	Low	No	Yes	No	−10.06	3
[b]5281642	302.24	7	5	131.36	1.99	Soluble	High	No	No	Yes	−6.60	0
[c]12443368	432.38	10	6	170.05	0.05	Soluble	Low	No	No	No	−8.33	1
[d]185617	341.44	3	1	47.56	4.52	Soluble	Low	No	Yes	No	−8.59	2
[e]5281605	270.24	5	3	90.90	2.58	Moderately soluble	High	No	No	Yes	−5.70	0

steps using the steepest descent and the conjugate gradient method. The system was gradually heated to 300 K using the Langevin thermostat. The SHAKE algorithm was employed for dealing with the hydrogen restraints. NPT equilibration was performed for 1ns at temperature of 300 K and 1atm pressure using Berendsen barostat. The production run was performed for 200ns using the NPT ensemble.

2.4. Analysis

All the simulation trajectories were analyzed for RMSD by cpptraj module of AMBERTOOLS20 [33]. The Molecular mechanics/Generalized Born Surface Area (MM-GBSA) free energy calculations were performed [34]. The MM-GBSA and Molecular Mechanics/Poisson-Boltzmann Surface Area (MM-PBSA) methods calculate binding free energies for macromolecules by combining molecular mechanics calculations and continuum solvation models.

$$\Delta G_{com/rec/lig} = \Delta H_{com/rec/lig} - T.\ \Delta S_{com/rec/lig}$$

$$<\Delta E^{gas}_{com/rec/lig}> + <\Delta G^{sol}_{com/rec/lig}> - T < \Delta S_{com/rec/lig}>$$

$$\Delta\Delta G_{bind} = \Delta G_{complex} - (\Delta G_{rec} + \Delta G_{lig})$$

Where $\Delta E^{gas}_{com/rec/lig}$ is a molecular mechanics energy for the complex, receptor and ligand. $\Delta G^{sol}_{com/rec/lig}$ is the solvation energy for the complex, receptor and ligand, which is calculated either by solving Poisson's equation or by using the Generalized Born solvation model. The ΔS is the entropy contribution. Snapshots were generated at 100ps intervals from the trajectories of 200ns length. These 500 snapshots were used to calculate the $\Delta\Delta G_{bind}$ of the complexes using the MMGBSA method (solvent dielectric constant = 78.5).

The non-bonded interactions (van der Waals and hydrogen bonding) between the ligand and the protein were calculated using the *GetContacts* module of FlarePlot [35]. The drug likeliness properties for the phytochemicals were calculated using the SwissADME tool [36]. The cluster analysis of the trajectories of best docked ligands on dUTPase and MDM2 were done using Ttclust tool [37].

3. Results and discussion

3.1. HPLC analysis of root bark extract

HPLC analysis of root and stem bark extract of *O. indicum* was conducted to check the presence of pharmacological molecules, and results showed the clear peaks of Baicalein (peak on retention time at 4 min) and Chrysin (peak on retention time at 19 min) in both extracts, comparable with standard of same molecules (Fig. 1). The observed quantity (w/w on plant dry weight basis) of baicalein in term of percentage was 0.13% while that of Chrysin was 0.09% in root bark extract. Similarly, content of baicalein and Chrysin in stem bark extract was found to be 0.64% and 0.04%, respectively.

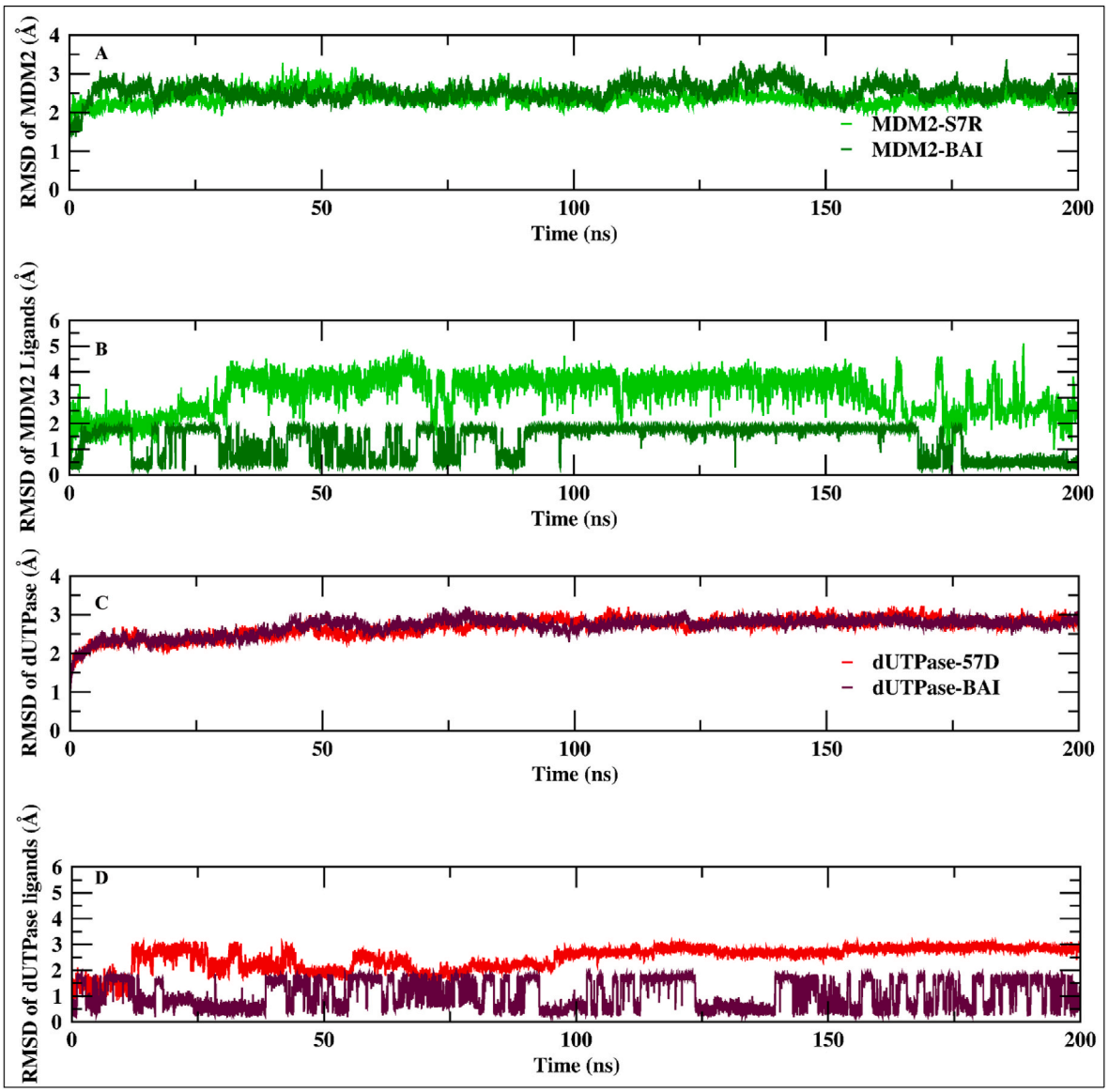

Fig. 5. RMSD of (A) MDM2, (B) MDM2-bound ligands in the MDM2-bound simulations and RMSD along the simulations of (C) dUTPase and (D) dUTPase-bound ligands in the dUTPase-bound simulations.

3.2. Molecular docking studies

The docking of the phytochemicals against three human (MDM2, EGFR, cyclooxygenase-2) and four viral (Uracil DNA glycosylase, NEC1, dUTPase, Bcl-2 homolog BHRF1) proteins (Table 4) was performed using the DOCK6 tool [27] and their corresponding scores are mentioned in Supplementary Table 1. The bar plot in Fig. 2 shows the docking scores for the best docked phytochemicals against these proteins. In case of the human proteins, the phytochemicals scutellarein 7-rutinoside (S7R), scutellarin (SCU) and 6-hydroxyluteolin (6HY) were observed to bind most favorably to MDM2, EGFR and cyclooxygenase-2, respectively. SCU was observed to bind to the viral protein uracil DNA glycosylase with best dock score. S7R was the best docked phytochemical to NEC1 and Bcl-2 homology BHRF1 viral proteins. dUTPase was observed to show most prominent binding to the phytochemical, 5, 7-Dihydroxy-2-phenyl-6-[3,4,5-trihydroxy-6-(hydroxymethyl) oxan-2-yl]oxychromen-4-one (57D). The docking scores for all of these molecules were found to be between −55 and −40 kcal/mol.

The Tanimoto similarity was also calculated between the phytochemicals BAI (Baicalein), 57D (Dihydroxy-2-phenyl-6-[3,4,5-trihydroxy-6-(hydroxymethyl)oxan-2-yl]oxychromen-4-one), S7R (scutellarein 7-rutinoside), 6HY (6-hydroxyluteolin), SCU (Scutellarin) from Shyonak (*Oroxylum indicum* Vent) with the known inhibitors (positive control ligands) of the respective target proteins viz 1F0 (MDM2), EBAI (BHRF1), Celecoxib (COX-2), Lapatinib (EGFR) as shown in Supplementary Fig. 2. The score of zero refers to no similarity while the score of 1 corresponds to 100% similarity. The similarity between MDM2's known inhibitor 1F0 with the *O. indicum* phytochemicals ranged from 0.35 to 0.91 while for other target protein's known inhibitors, the similarity with *O. indicum* phytochemicals was lower ranging from 0.095 to 0.49.

3.3. Docking of baicalein

Fig. 3 shows the docking of Baicalein against the seven proteins. The bar plot in Fig. 3 shows the grid scores obtained in each of the human and viral protein targets considered. It was observed that in case of viral proteins the docking score ranged within −37 to −28 kcal/mol dUTPase showed the lowest value of docking score suggesting most stable binding with Baicalein. In case of the human proteins, cyclooxygenase-2 showed a docking score in the similar range.

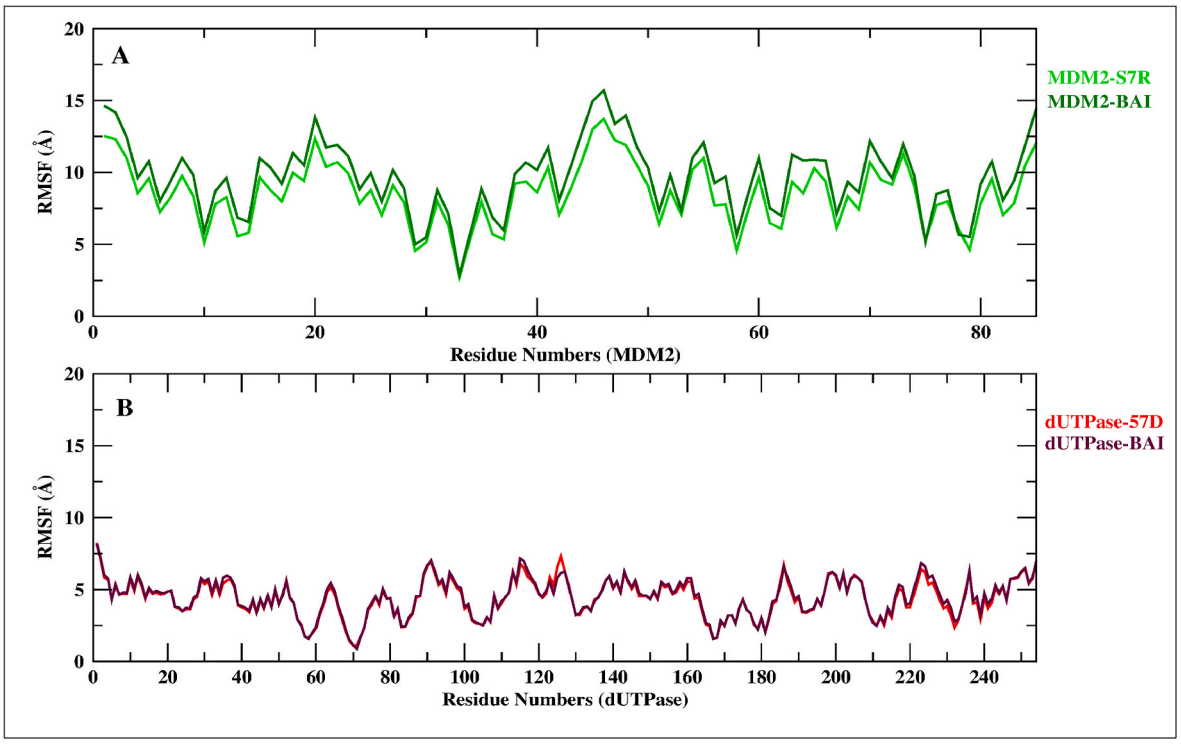

Fig. 6. RMSF of MDM2 in MDM2-bound ligands complex and dUTPase in dUTPase-bound ligands complex over the 200ns simulations.

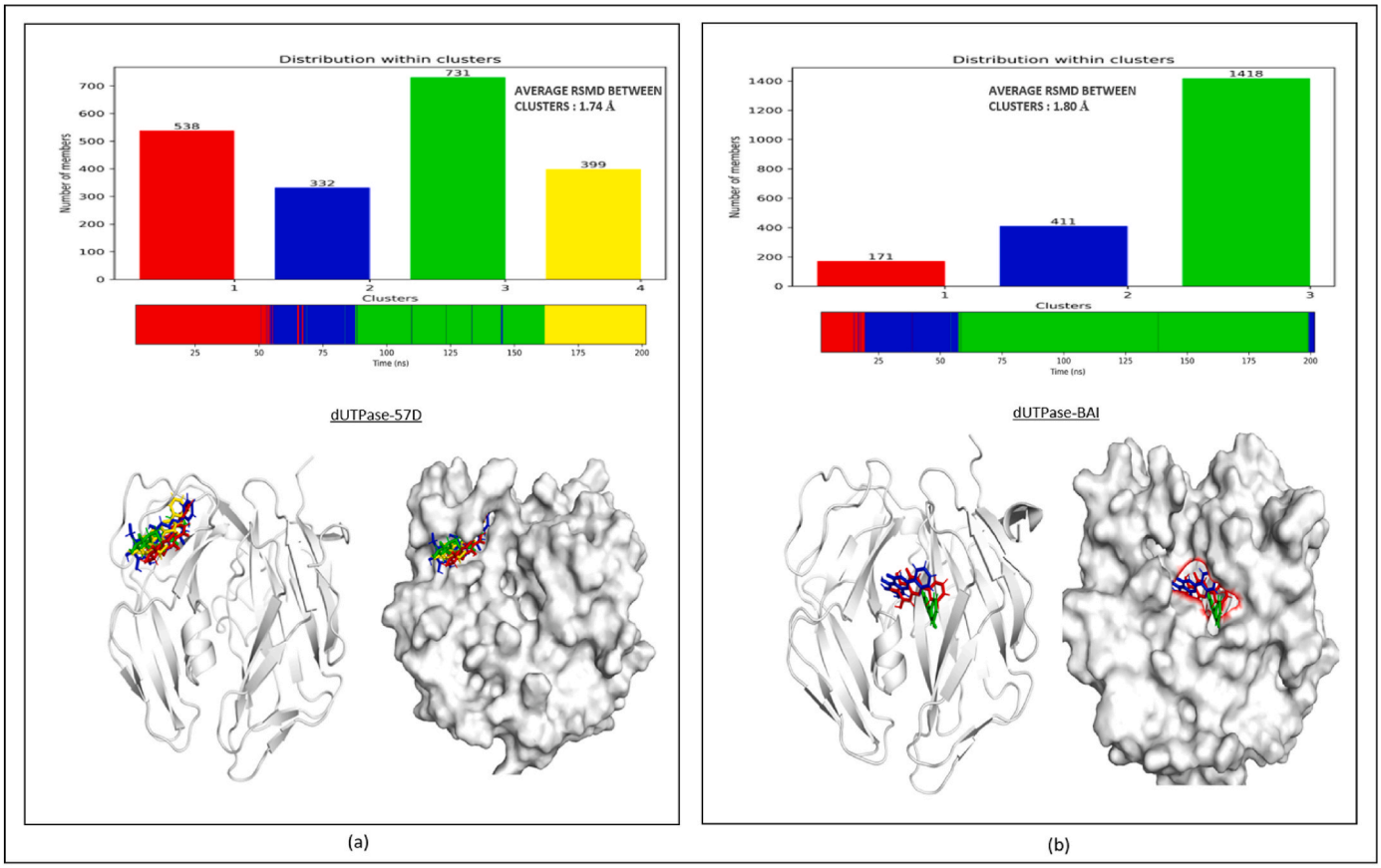

Fig. 7. Cluster analysis of (A) dUTPase-57D complex and (B) dUTPase-BAI complex and their corresponding representative structures over the 200ns simulations. The average RMSD between the clusters in each complex was found to be 1.74 Å and 1.80 Å respectively.

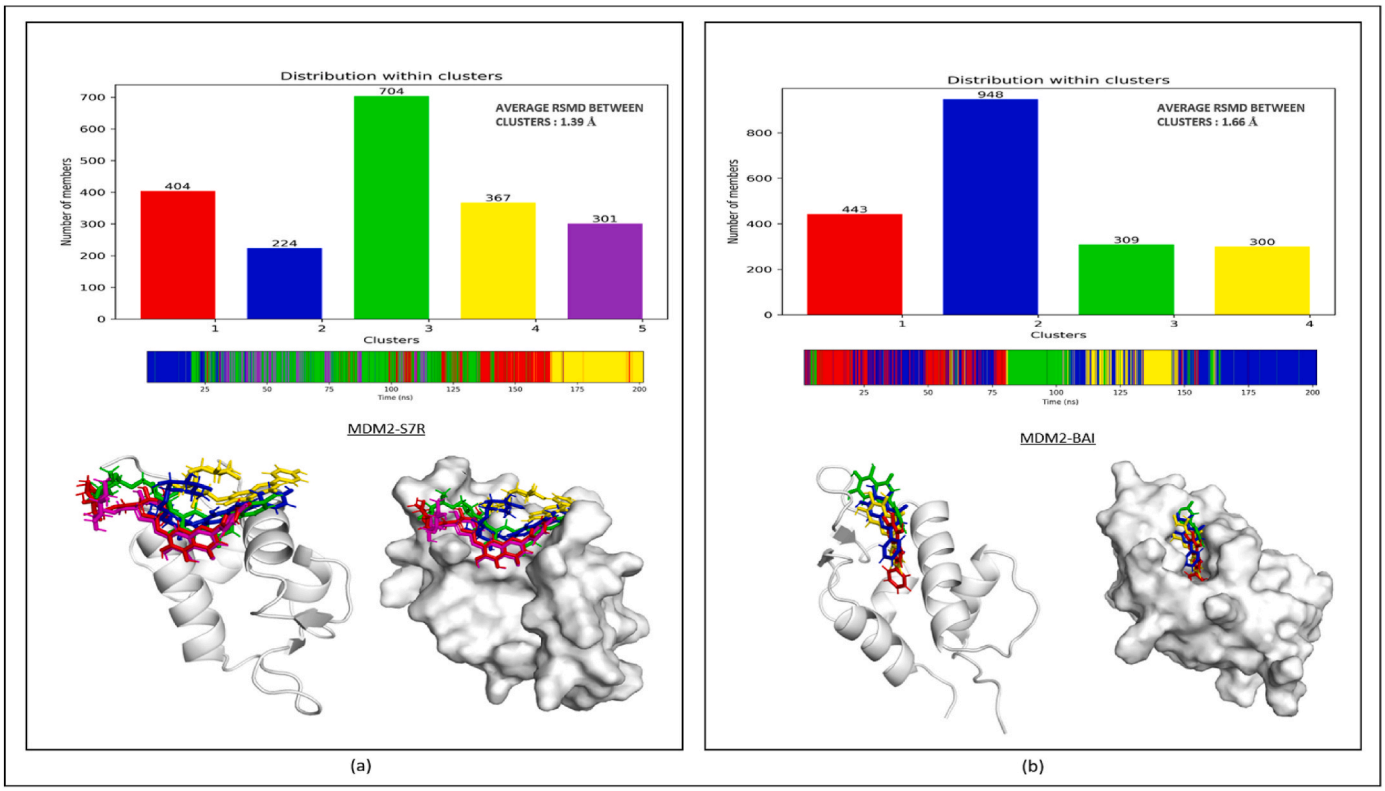

Fig. 8. Cluster analysis of (A) MDM2-S7R complex and (B) MDM2-BAI complex and their corresponding representative structures over the 200ns simulations. The average RMSD between the clusters in each complex was found to be 1.39 Å and 1.66 Å respectively.

3.4. Validation of docking protocol

The co-crystal docking of MDM2 (PDB ID: 4IPF) was performed using DOCK6 [27]. The crystal structure of MDM2 consisted of the ligand RO5045337 (PubChem ID: 57,406,853). This ligand was docked on to the MDM2 structure using the docking protocol discussed in the methodology section. Fig. 4 shows the superimposition of the docked ligand (pink) on to the crystal position (blue) of the ligand in PDB ID: 4IPF. It was observed that the all atom RMSD was 1.8 Å, which suggests near to the crystal position for the ligand.

3.5. Drug likeliness of phytochemicals

The drug likeliness properties of the five phytochemicals (Table 5), namely, S7R, SCU, 57D, 6HY and BAI were studied using the SwissADME server [36]. The parameters calculated for understanding the drug likeliness suggested that most of the parameters were lying well in the allowed limits for small molecules that can be considered for further studies of drug development.

3.6. Conformational dynamics of protein-ligand complexes

3.6.1. Overall dynamics

The molecular dynamics simulations were performed for the human protein (MDM2) and EBV protein (dUTPase). Total of four simulations were performed, namely, MDM2-S7R, MDM2-BAI, dUTPase-57D and dUTPase-BAI. S7R was found to be the best docked phytochemical for MDM2 while 57D was found to be the best docked phytochemical for dUTPase.

As this study focused on Baicalein (BAI) hence, the Baicalein docked structures of MDM2 and dUTPase were also studied through simulations. The trajectory of 200ns were divided into four blocks of 50ns each and plotted the block RMSD considering the average structure of the block as the reference structure to calculate the block RMSD as shown in Supplementary Fig. 1. The block RMSD was appeared to maintain stable values around 1.5 to 2 Å for the proteins MDM2 (Supplementary Fig. 1A) and dUTPase (Supplementary Fig. 1 C) in both the ligand bound systems in all the four blocks. The block RMSD showed overall convergence of the protein-ligand complex system over the simulation run. Fig. 5 shows the root mean square deviation values for these simulations considering the start structure of the simulation as the reference. Fig. 5A shows the RMSD of MDM2 in the MDM2-S7R and MDM2-BAI simulation systems. It was observed that throughout the 200ns of the simulation time, MDM2 was stable within 2-3Å. However, the ligands S7R and BAI appeared to fluctuate significantly in the MDM2-S7R and MDM2-BAI systems, respectively (Fig. 5B). In case of S7R, the RMSD was observed to increase fluctuate between 2.5 Å and 4 Å in the last 200ns (Fig. 5B). BAI was observed to span within two RMSD values, namely, 0.5 Å and 1.5 Å at distinct simulation times (Fig. 5B).

Fig. 5C showed the RMSD of dUTPase in the dUTPase-57D and dUTPase-BAI simulation systems. It was observed that throughout the simulation time dUTPase was stable around RMSD value of 2.5 Å in the presence of either 57D or BAI. Similar to MDM2-ligand complexes, the ligands 57D and BAI were observed to fluctuate significantly (Fig. 5D). The ligand 57D was observed to maintain stability at the 3 Å for almost the entire simulation time. However, in case of BAI the RMSD values were between 0-1Å for majority of the simulation time. The maximum RMSD reached by BAI was around 1.5 Å.

Residue-wise Root Mean Square Fluctuation (RMSF) (Fig. 6) was calculated for MDM2 residue when bound to S7R and BAI. It was observed that the fluctuations were quite similar in the presence of either of the ligand-bound states. Similarly, in the case of dUTPase too, the fluctuations for its residues were almost lying within the same RMSF range in the presence of either of the ligands.

The cluster analysis of the MD trajectories was done using Ttclust tool. Top clusters of protein-ligand complexes identified over the

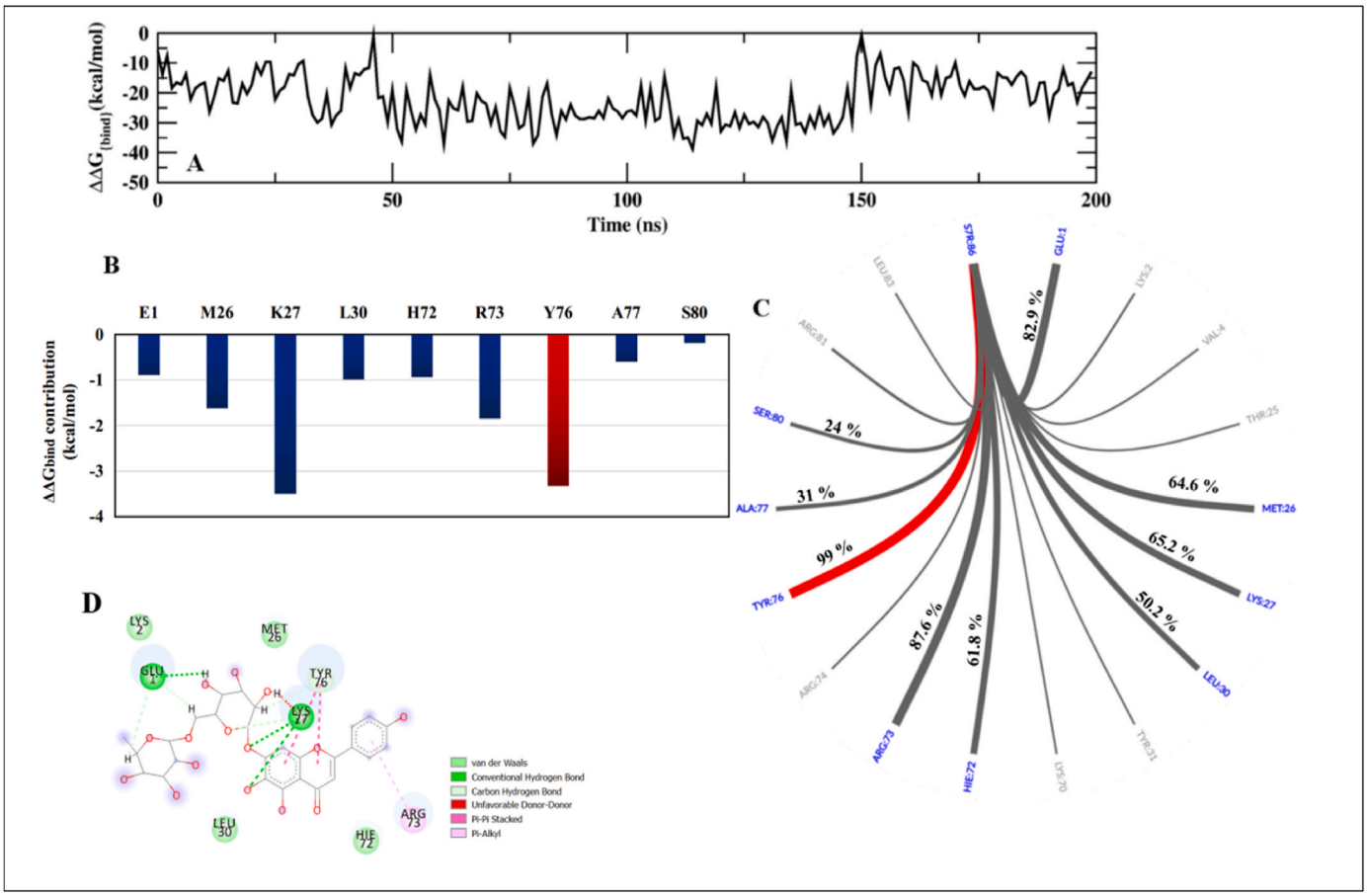

Fig. 9. (A) $\Delta\Delta G_{bind}$ between MDM2 and S7R for the MDM2-S7R simulations. (B) Free energy contribution in binding between MDM2 and S7R for the MDM2 residues forming non-bonded interactions with S7R. (>90% marked in red) (C) Non-bonded interactions between MDM2 residues and S7R along with their percentage occupancy (>90% marked in red). (D) 2D representation of the interactions between MDM2 and S7R.

trajectories are shown in Figs. 7 and 8. Fig. 7A shows four distinct clusters of dUTPase-57D complex with the average RMSD of 1.74 Å while Fig. 7B shows three clusters of dUTPase-BAI complex with the average RMSD of 1.80 Å. In the case of MDM2-ligand complexes, the MDM2-S7R complex (Fig. 8A) showed up to five clusters with an average RMSD of 1.39 Å between the representative structures while MDM2-BAI complex (Fig. 8B) showed four clusters with an average RMSD of 1.66 Å between the clusters. Based on the average RMSD values of each cluster in the respective protein-ligand complexes, the systems were found to be stable and converged.

Hence, the overall dynamics suggest that, the protein as whole acted similar in presence of the best docked phytochemical and BAI for both MDM2 and dUTPase. The stability of the best docked phytochemical appeared to be less as compared to the BAI in case of MDM2. This may suggest that even though BAI ranked lower in terms of the docking score it showed comparatively lower RMSD values inferring better stability than the top ranked phytochemical.

3.6.2. *Interactions with best docked phytochemicals*

The average binding energy values of the S7R with MDM2 and 57D with dUTPase with the decomposition of energy components are shown in the Supplementary Table 2. Figs. 9 and 10 shows the binding between S7R with MDM2 and 57D with dUTPase, respectively. Fig. 9A shows the ΔΔGbind between S7R and MDM2 for entire 200 ns of the simulation time, the calculations were performed at every ns. The free energy of binding was observed to lie between −30 and −10 kcal/mol. In order to dig deeper into the binding between the two, the residue-wise free energy contribution in binding (Fig. 9B) and percentage occupancy of non-bonded interactions (van der Waals and hydrogen bonding) between S7R and MDM2 (Fig. 9C) were calculated, respectively. The residues showing an occupancy of more than 20 % have been shown in Fig. 9B and C. E1, M26, K27, L30, H72, R73, Y76, A77 and S80 were observed to interact with S7R. It was observed that Y76 showed most contribution in binding attributing to the most stable free energy contribution (−3.3 kcal/mol) and highest percentage occupancy (99 %) of the non-bonded interactions.

Fig. 10 shows binding parameters for the dUTPase-57D simulation. Fig. 10A shows the $\Delta\Delta G_{bind}$ between 57D and dUTPase for entire 200 ns of the simulation time, the calculations were performed at every ns. It was observed that the $\Delta\Delta G_{bind}$ was improving by the end of the simulation, ranging between −40 and −30 kcal/mol. The residues T111, N122, H123, P124, Q125, Y126, P127, G128, D129, V130, G131, L132, D133, and R208 were observed to interact with the ligand 57D (Fig. 10B). D133 was observed to contribute the most in terms of the free energy of binding. This residue showed percentage occupancy of 96.4 % in forming interactions with 57D (Fig. 10C). Y126, L132 and R208 all showed comparatively better contribution in free energy of binding. This was complimented with high percentage occupancy of interactions with 57D, calculated around 84.4 %, 60.1 % and 92.9%, respectively. The residues contributing significantly to the free energy binding with 57D were observed to form strong non-bonded interactions with the ligand throughout the simulation. Three residues, namely D129, D133 and R208 were observed to form non-bonded interactions with more than 90 % of percentage occupancy.

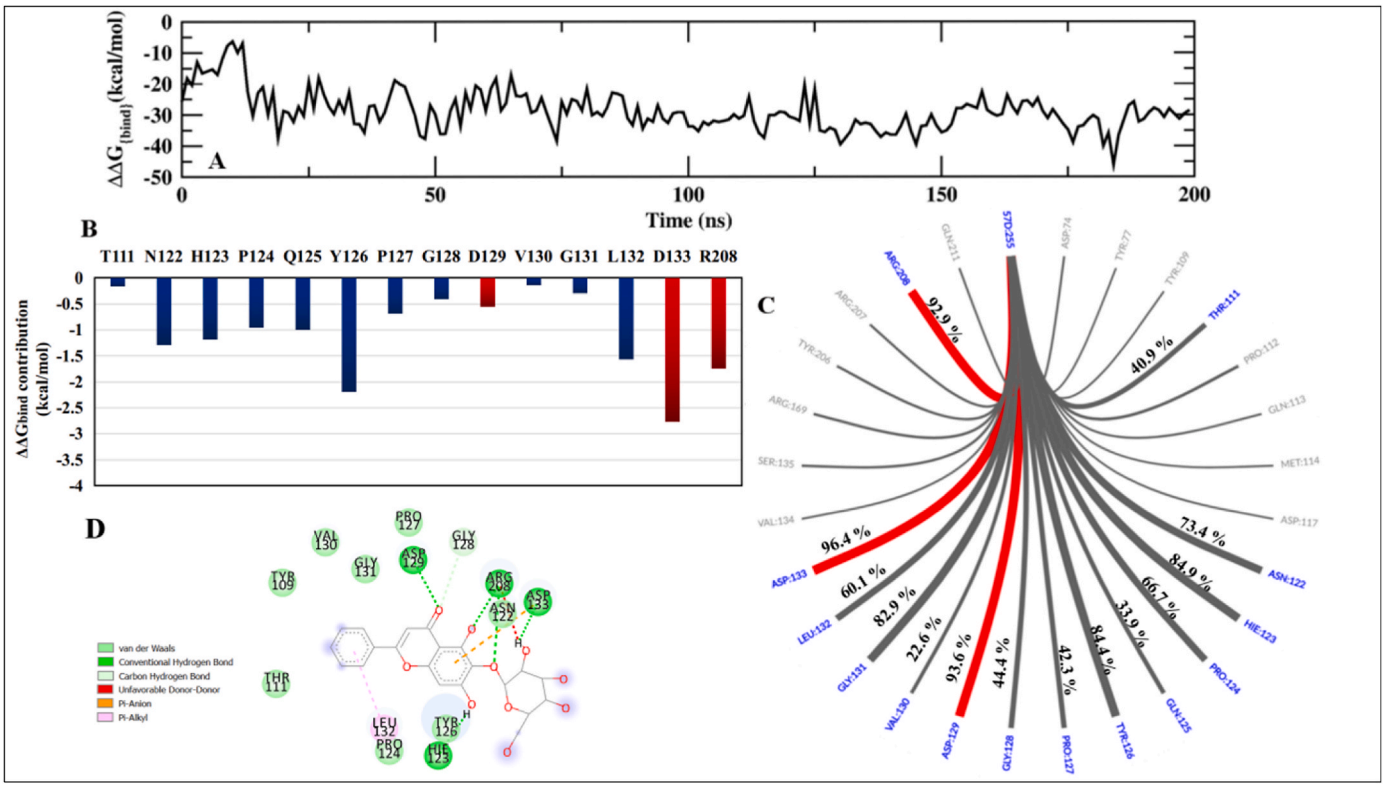

Fig. 10. (A) $\Delta\Delta G_{bind}$ between dUTPase and 57D for the dUTPase-57D simulations. (B) Free energy contribution in binding between dUTPase and 57D for the dUTPase residues forming non-bonded interactions with 57D. (>90% marked in red) (C) Non-bonded interactions between dUTPase residues and 57D along with their percentage occupancy. (>90% marked in red). (D) 2D representation of the interactions between dUTPase and 57D.

3.6.3. *Interactions with baicalein*

The average binding energy values of the BAI with MDM2 and dUTPase with the decomposition of energy components are shown in the Supplementary Table 2. Figs. 11 and 12 shows the interaction of MDM2 and dUTPase with baicalein in terms of free energy of binding, residue-wise contribution in free energy binding and percentage occupancy of non-bonded interactions formed between the protein and ligand, respectively. Fig. 11A depicts that the $\Delta\Delta G_{bind}$ was stable within −30 to −20 kcal/mol between BAI and MDM2. The free energy contribution by the residues of MDM2 has been shown in Fig. 11B. G34, I37, M38, Y43, D44, Q47, Q48, H49, I50, V51 and V69 were observed to contribute in free energy of binding with BAI. Y43 was observed to contribute the most; also the percentage occupancy of this residue was 99.7%. This was the strongest binding residue in terms of free energy contribution and percentage occupancy of interactions formed with BAI. Q47, Q48, and I50 showed percentage occupancy of more than 90%. I50 was the second most contributing residue in terms of the free energy of binding to BAI as shown in Fig. 11C. This suggests that these interactions remained stable throughout the simulation length. Additionally, on comparing the $\Delta\Delta G_{bind}$ of MDM2 with BAI and S7R, it was observed that MDM2 showed stable binding to BAI than S7R.

Fig. 12A shows the ΔΔGbind between dUTPase and BAI, which was stable between −30 and −20 kcal/mol. The residues L58, H69, G71, I72, I73, Y77, R82, L83, I84, G168, S170, M174 and Q211 were observed to form interaction with BAI, Fig. 12B shows the contribution of these residues in the free energy of binding. Fig. 12C depicts the percentage occupancy of interactions formed by these residues with BAI. I73 was observed to contribute the most in the free energy of binding, however, the percentage occupancy of this interaction was round 52.9%. In terms of percentage occupancy of the interaction formed with BAI, three residues, namely, H69, I72 and S170 showed a percentage occupancy of more than 85 %. This indicates that these interactions were maintained throughout the simulation length.

4. Discussion

This study explored *Oroxylum indicum* (Shyonaka), which is traditionally used in several ethnomedicinal systems to treat various human ailments. Our study identified potential dual targeting inhibitors from selected plant for EBV and NPC along with quantification analysis of root and stem bark, for confirming the presence of prevalent phytochemicals, Baicalein and Chrysalin. Various reports are available for application of these phytochemicals obtained from this plant in nasopharyngeal, oral and breast cancers [16,38].

Our study attempted molecular dynamics simulations of S7R and Baicalein, with human protein (MDM2), and 57D, Baicalein, with viral protein dUTPase, and attained stable interactions between them. This was also confirmed by the binding energy calculations. Buranrat et al. [16] had observed inhibition of cell proliferation in breast cancer cells using *O. indicum* extracts prepared from leaves and fruits. They also claimed reduction in expression of cell cycle regulatory protein, Rac1. Moreover, another group [39] evaluated cytotoxic effects of ethanol extracts of *O. indicum* on HeLa cells and observed induction of apoptosis and suppressed levels of NF-κB, COX-2, Nrf2, and RASSF7 proteins. Rajkumar et al. [40] reported induction of apoptosis in MDA-MB-435 S (human breast carcinoma), Hep3B (human hepatic carcinoma), and PC-3 (human prostate cancer) cell lines upon treatment with aqueous and methanolic extracts of stem bark of *O. indicum*.

Above reports and reviews suggested that various phytochemical constituents present in *O. indicum* can be explored for their different pharmacological applications especially pertaining to cancer treatments.

The two phytochemicals S7R and SCU appeared to be promising as they were found to bind with best docking score to human and viral proteins. In case of S7R, it bound the best to MDM2, which is a crucial protein in the p53-dependent cancer pathway. The inhibition of MDM2 leads to increased concentration of tumor suppressor p53, which further

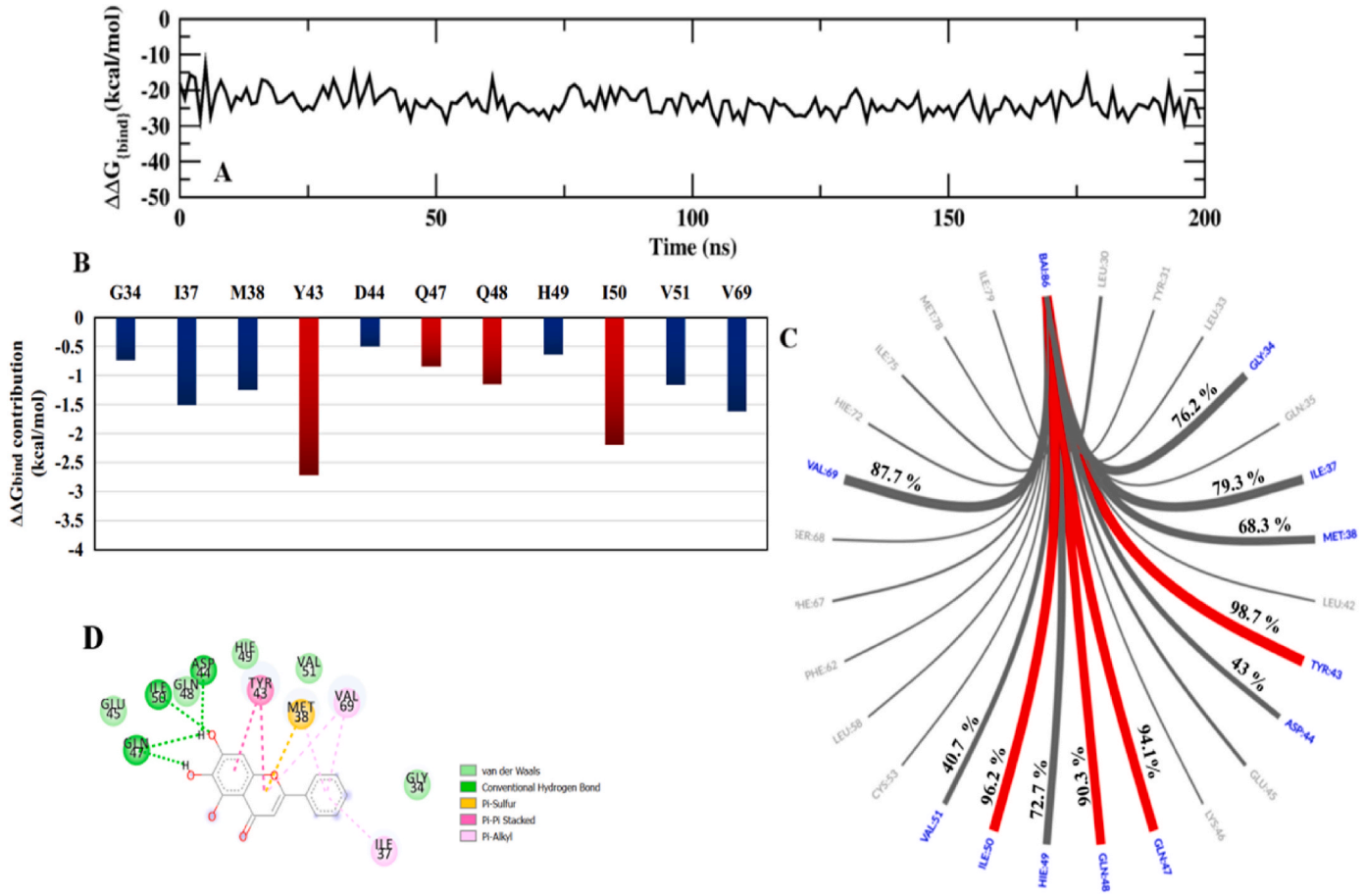

Fig. 11. (A) $\Delta\Delta G_{bind}$ between MDM2 and BAI for the MDM2-BAI simulations. (B) Free energy contribution in binding between MDM2 and BAI for the MDM2 residues forming non-bonded interactions with BAI. (>90% marked in red) (C) Non-bonded interactions between MDM2 residues and BAI along with their percentage occupancy. (>90% marked in red). (D) 2D representation of the interactions between MDM2 and BAI.

performs its function to express genes that transcribe proteins that halt tumor progression in cancer. SCU was observed to be the best docked ligand for the EGFR (human) and uracil DNA glycosylase (viral). The former being one of the crucial proteins in human cancers. Whereas, the latter one is crucial for viral growth.

Previous studies have showed the potential of Baicalein in the prevention and treatment of nasopharyngeal and oral cancers, in various cell line models [41–43]. Similarly, this in-silico study identified the strong and stable binding of Baicalein to the target proteins of EBV and NPC which were previously not reported to bind with Baicalein.

On this basis, the in-silico evaluation of the selected phytochemicals from *O. indicum* conducted in our study, with target proteins indicated their potential to inhibit both EBV and NPC. This study will pave way for further in-vitro and in-vivo validations using these phytochemicals.

5. Conclusions

Based on the literature, many studies have showed the association of EBV with NPC. This study is focused to identify the role of *Oroxylum indicum* in the dual inhibition of NPC and EBV. The screened compounds from *Oroxylum indicum* are binding with high affinity to the target proteins involved in EBV and NPC. Based on the docking score, molecular dynamics simulations and binding energy calculations, the phytochemicals S7R, SCU and Baicalein are binding with high affinity to the target proteins MDM2 and dUTPase. Out of these, Baicalein showed better binding to MDM2 than S7R, however, the binding with dUTPase was comparable with 57D. Based on these results, we propose the dual inhibitory activity of phytochemicals from *Oroxylum indicum* against EBV and NPC. However, the validation of binding of these screened compounds to the target proteins needs to be done using in vitro surface plasmon resonance and isothermal calorimetric analysis, followed by in vitro cell line and in vivo mouse models testing before moving to the clinical trials.

Funding

The authors are also thankful to CCRAS for providing the required funding and infrastructure to carry out this study.

CRediT author statement

SRT and GS: conceptualization and supervision, docking, writing, reviewing, compiling, and editing.

HS, ST: reviewing, writing and editing.

SK, MVNU, VJ, US and RJ: High Performance Computing (HPC) based In-Silico Study, editing and writing.

YG, VK and SKM: HPLC analysis, reviewing and writing.

VC, MC, RN, VL, CVN, NS, RA: Ayurveda literature, analysis, discussion, drafting and supervision.

Declaration of generative AI and AI-assisted technologies in the writing process

None.

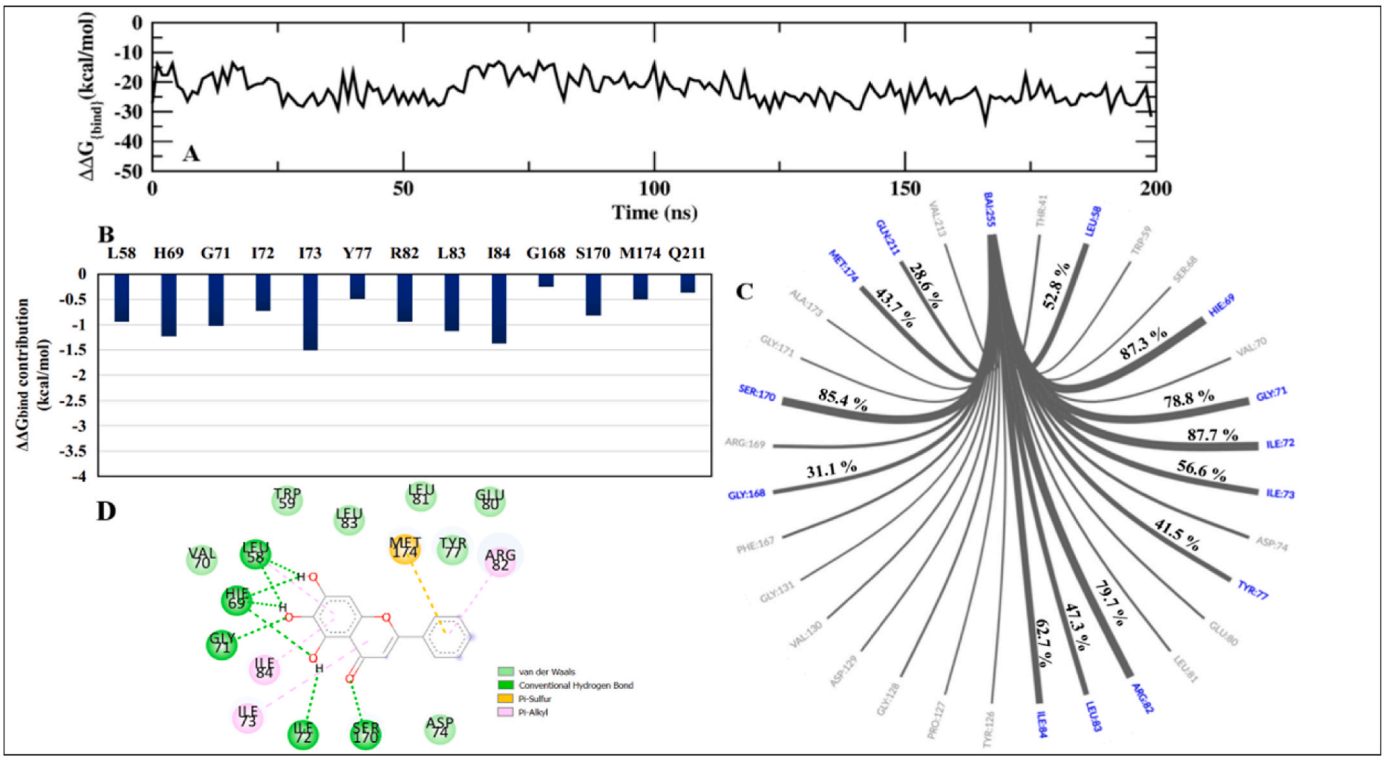

Fig. 12. (A) $\Delta\Delta G_{bind}$ between dUTPase and BAI for the dUTPase-BAI simulations. (B) Free energy contribution in binding between dUTPase and BAI for the dUTPase residues forming non-bonded interactions with BAI. (C) Non-bonded interactions between dUTPase residues and BAI along with their percentage occupancy. (D) 2D representation of the interactions between dUTPase and BAI.

Declaration of competing interest

The authors declare that they have no known competing financial interests or personal relationships that could have appeared to influence the work reported in this paper.

Acknowledgements

The authors acknowledge the botanists Dr. J.C. Arya and Mr. Virendra Singh for validating and providing the accession number for the *Oroxylum indicum* Vent collected from the garden of Central Ayurveda Research Institute Jhansi.

Appendix A. Supplementary data

Supplementary data to this article can be found online at https://doi.org/10.1016/j.jaim.2024.100986.

References

[1] Mao AA. Oroxylum indium Vent. - a potential anticancer medicinal plant. Indian J Tradit Knowl 2002;1(1):17–21.
[2] Jagetia GC. A review on the medicinal and pharmacological properties of traditional ethnomedicinal plant sonapatha. Oroxylum indicum Sinusitis 2021;5(1):71–89. https://doi.org/10.3390/sinusitis5010009.
[3] The Ayurvedic Pharmacopoeia of India. Part III. first ed.. Department of Indian system of medicine and homoeopathy, Ministry of Health and Family Welfare, Government of India. p. 210..
[4] Sharma PV. Classical uses of medicinal plants. Varanasi: Chaukhambha Visvabharati; 1996.
[5] Sharma PV. Dravyaguna vijnana. Reprinted, vol. II. Varanasi, India: Chaukhamba Bharati Academy; 2009.
[6] Bhāvamiśra. Bhāvaprakāśanighaṇṭu. Reprinted. In: Chunekar GPKC, editor. Varanasi. Chaukhambha bharathi academy, varanasi; 1998.
[7] Kaiyadevanighantu E-Nighantu. National Institute of Indian medical heritage (NIIMH). Hyderabad; 2012.
[8] Dhanvantarinighantu E-Nighantu. National Institute of Indian medical heritage (NIIMH). Hyderabad; 2012.
[9] Madanapalanighantu E-Nighantu. National Institute of Indian medical heritage (NIIMH). Hyderabad; 2012.
[10] Madanadinighantu E-Nighantu. National Institute of Indian medical heritage (NIIMH). Hyderabad; 2012.
[11] Rajavallabhanighantu E-Nighantu. National Institute of Indian medical heritage (NIIMH). Hyderabad; 2012.
[12] Rajanighantu E-Nighantu. National Institute of Indian medical heritage (NIIMH). Hyderabad; 2012.
[13] N. D. Ministry of Ayush, Standardized ayurvedic terminologies (SAT). National ayush morbidity and standardized terminologies electronic (NAMASTE) portal, ..
[14] W. H. Organization. WHO international standard terminologies on ayurveda. 2022.
[15] Sharmila KP, Shilpa SS, Kumari S, Madhyastha H, Ashwini P, Satheesh Kumar Bhandary B. Oroxylum indicum stem bark extract exerts antitumor potential against Ehrlich's ascites carcinoma in Swiss albino mice. Biomedicine 2022;42(4):686–92. https://doi.org/10.51248/.v42i4.1559.
[16] Buranrat B, Noiwetch S, Suksar T, Ta-Ut A. Inhibition of cell proliferation and migration by Oroxylum indicum extracts on breast cancer cells via Rac1 modulation. J Pharm Anal 2020;10(2):187–93. https://doi.org/10.1016/j.jpha.2020.02.003.
[17] Prakash O, Kumar A, Kumar P, Ajeet A. Anticancer potential of plants and natural products: a review. Am J Pharmacol Sci 2013;1(6):104–15. https://doi.org/10.12691/ajps-1-6-1.
[18] Kumar Kr VD. 100 red listed medicinal plants of conservation concern in southern India. Bangalore, India: Foundation for Revitalisation of Local Health Traditions.; 2000. p. 1–467.
[19] Su ZY, Siak PY, Leong CO, Cheah SC. The role of Epstein-Barr virus in nasopharyngeal carcinoma. Front Microbiol 2023;14:1116143. https://doi.org/10.3389/fmicb.2023.1116143.
[20] Al-Anazi AE, Alanazi BS, Alshanbari HM, Masuadi E, Hamed ME, Dandachi I, Alkathiri A, Hanif A, Nour I, Fatani H, Alsaran H, Alkhareeb F, Al Zahrani A, Alsharm AA, Eifan S, Alosaimi B. Increased prevalence of EBV infection in nasopharyngeal carcinoma patients: a six-year cross-sectional study. Cancers 2023;15(3). https://doi.org/10.3390/cancers15030643.
[21] Guidry JT, Birdwell CE, Scott RS. Epstein-Barr virus in the pathogenesis of oral cancers. Oral Dis 2018;24(4):497–508. https://doi.org/10.1111/odi.12656.
[22] Sung H, Ferlay J, Siegel RL, Laversanne M, Soerjomataram I, Jemal A, Bray F. Global cancer statistics 2020: GLOBOCAN estimates of incidence and mortality worldwide for 36 cancers in 185 countries. CA A Cancer J Clin 2021;71(3):209–49. https://doi.org/10.3322/caac.21660.
[23] W. H. Organization, Malignant neoplasms of nasopharynx (2B6B). ICD-11 for mortality and morbidity statistics (Version : 01/2023)..
[24] IMPPAT: Indian Medicinal Plants, Phytochemistry And Therapeutics. Retrieved on June 25, 2023, from https://cb.imsc.res.in/imppat/phytochemical/Oroxylum%20indicum..

[25] Rai D, Aswatha Ram HN, Neeraj Patel K, Babu UV, Sharath Kumar LM, Kannan R. In vitro immuno-stimulatory and anticancer activities of Oroxylum indicum (L.) Kurz.: an evidence for substitution of aerial parts for conservation. J Ayurveda Integr Med 2022;13(2):100523. https://doi.org/10.1016/j.jaim.2021.09.001.
[26] Yadav AK, Manika N, Bagchi GD, Gupta MM. Simultaneous determination of flavonoids in Oroxylum indicum by RP-HPLC. Med Chem Res 2012;22(5):2222–7. https://doi.org/10.1007/s00044-012-0214-8.
[27] Allen WJ, Balius TE, Mukherjee S, Brozell SR, Moustakas DT, Lang PT, Case DA, Kuntz ID, Rizzo RC. Dock 6: impact of new features and current docking performance. J Comput Chem 2015;36(15):1132–56. https://doi.org/10.1002/jcc.23905.
[28] Pettersen EF, Goddard TD, Huang CC, Couch GS, Greenblatt DM, Meng EC, Ferrin TE. UCSF Chimera–a visualization system for exploratory research and analysis. J Comput Chem 2004;25(13):1605–12. https://doi.org/10.1002/jcc.20084.
[29] Tian C, Kasavajhala K, Belfon KaA, Raguette L, Huang H, Migues AN, Bickel J, Wang Y, Pincay J, Wu Q, Simmerling C. ff19SB: amino-acid-specific protein backbone parameters trained against quantum mechanics energy surfaces in solution. J Chem Theor Comput 2020;16(1):528–52. https://doi.org/10.1021/acs.jctc.9b00591.
[30] Case KBDA, Ben-Shalom IY, Brozell SR, Cerutti DS, Cheatham Iii TE, Cruzeiro VWD et al. Amber 2020. San Francisco: University of California; 2020.
[31] Wang J, Wolf RM, Caldwell JW, Kollman PA, Case DA. Development and testing of a general amber force field. J Comput Chem 2004;25(9):1157–74. https://doi.org/10.1002/jcc.20035.
[32] Wang J, Wang W, Kollman PA, Case DA. Automatic atom type and bond type perception in molecular mechanical calculations. J Mol Graph Model 2006;25(2):247–60. https://doi.org/10.1016/j.jmgm.2005.12.005.
[33] Roe DR, Cheatham TE. Parallelization of CPPTRAJ enables large scale analysis of molecular dynamics trajectory data. J Comput Chem 2018;39(25):2110–7. https://doi.org/10.1002/jcc.25382.
[34] Miller 3rd BR, Mcgee Jr TD, Swails JM, Homeyer N, Gohlke H, Roitberg AE. MMPBSA.py: an efficient program for end-state free energy calculations. J Chem Theor Comput 2012;8(9):3314–21. https://doi.org/10.1021/ct300418h.
[35] Getcontacts. Available from: https://getcontacts.github.io/.
[36] Daina A, Michielin O, Zoete V. SwissADME: a free web tool to evaluate pharmacokinetics, drug-likeness and medicinal chemistry friendliness of small molecules. Sci Rep 2017;7:42717. https://doi.org/10.1038/srep42717.
[37] Tubiana T, Carvaillo J-C, Boulard Y, Bressanelli S. TTClust: a versatile molecular simulation trajectory clustering program with graphical summaries. J Chem Inf Model 2018;58(11):2178–82. https://doi.org/10.1021/acs.jcim.8b00512.
[38] Verma E, Kumar A, Devi Daimary U, Parama D, Girisa S, Sethi G, Kunnumakkara AB. Potential of baicalein in the prevention and treatment of cancer: a scientometric analyses based review. J Funct Foods 2021;86. https://doi.org/10.1016/j.jff.2021.104660.
[39] Lalrinzuali K, Vabeiryureilai M, Jagetia GC. Sonapatha (Oroxylum indicum) mediates cytotoxicity in cultured HeLa cells by inducing apoptosis and suppressing NF-κB, COX-2, RASSF7 and NRF2. Bioorg Chem 2021;114. https://doi.org/10.1016/j.bioorg.2021.105126.
[40] Rajkumar V, G G, Ashok Kumar R. Induction of apoptosis in MDA-MB-435S, Hep3B and PC-3 cell lines by extracts of Oroxylum indicum. J Pharm Res 2011;4(7):2054–6.
[41] Zhang Y, Wang H, Liu Y, Wang C, Wang J, Long C, Guo W, Sun X. Baicalein inhibits growth of Epstein-Barr virus-positive nasopharyngeal carcinoma by repressing the activity of EBNA1 Q-promoter. Biomed Pharmacother 2018;102:1003–14. https://doi.org/10.1016/j.biopha.2018.03.114.
[42] Guo J, You H, Li D. Baicalein exerts anticancer effect in nasopharyngeal carcinoma in vitro and in vivo. Oncol Res 2019;27(5):601–11. https://doi.org/10.3727/096504018X15399945637736.
[43] Cheng YH, Li LA, Lin P, Cheng LC, Hung CH, Chang NW, Lin C. Baicalein induces G1 arrest in oral cancer cells by enhancing the degradation of cyclin D1 and activating AhR to decrease Rb phosphorylation. Toxicol Appl Pharmacol 2012;263(3):360–7. https://doi.org/10.1016/j.taap.2012.07.010.